A ^{210}Pb-based chronological model for recent sediments with random entries of mass and activities: Model development

José-María Abril Hernández

Departamento de Física Aplicada I, ETSIA Universidad de Sevilla, Carretera de Utrera km 1; D.P. 41013 Seville, Spain

Keywords:

^{210}Pb dating
Sediment dating
Random SAR
Random initial activity
TERESA model

A B S T R A C T

Unsupported ^{210}Pb (^{210}Pb$_{exc}$) vs. mass depth profiles do not contain enough information as to extract a unique chronology when both, ^{210}Pb$_{exc}$ fluxes and mass sediment accumulation rates (SAR) indepen-dently vary with time. Restrictive assumptions are needed to develop a suitable dating tool. A statistical correlation between fluxes and SAR seems to be a quite general rule. This paper builds up a new ^{210}Pb-based dating tool by using such a statistical correlation. It operates with SAR and initial activities that closely follow normal distributions, what leads to the expected correlation between fluxes and SAR. An intelligent algorithm solves their best arrangement downcore to fit the experimental ^{210}Pb$_{exc}$ vs. mass depth profile, generating then solutions for the chronological line, and for the histories of SAR and fluxes. Parametric maps of a χ-function serve to find out the solution and to support error estimates. Optionally, the model's answers can be better constrained through the use of time markers. The performance of the model is illustrated with a synthetic core, and with real cases using published data for varved sediment cores.

1. Introduction

Without accurate methods of dating recent sediment cores it is not possible to provide a quantitative description of sediment accumulation rate (SAR) and deposition processes, which are the key for reconstructing past environmental conditions. High resolution chronologies are possible for sediments with varves, but they rarely occur in most sedimentary sequences (Ojala et al., 2012). The radiometric dating is the only technique of general applicability that claims to provide an absolute age determination (Carroll and Lerche, 2003).

The most common technique for dating recent sediments uses fallout ^{210}Pb, a natural radionuclide (see the reviews by Appleby, 2008; Sánchez-Cabeza and Ruíz-Fernández; 2010; Mabit et al., 2014). In recent years the combined use of ^{210}Pb and some bomb-fallout radionuclides (e.g., ^{137}Cs, ^{241}Am and $^{239+240}$Pu) has been widely popularized in the radiometric dating of recent sediments, accounting for one of the most interesting applications of the environmental radioactivity.

Abril (2015) has shown that under the assumptions of continuity of the sequence, ideal deposition of ^{210}Pb$_{exc}$ fluxes, and non post-depositional redistribution, any ^{210}Pb$_{exc}$ activity versus mass depth profile, even with the restriction of a discrete set of time markers (reference points), is compatible with an infinite number of chronological lines. Consequently, there are an infinite number of mathematically exact solutions for histories of initial activity, SAR and flux onto the sediment to water interface (SWI). Such histories may contain values of SAR and flux ranging from zero up to infinity. Thus, the development of a suitable dating tool is not possible without the explicit introduction of restrictive assumptions about flux, SAR and/or their interrelationship. These may be the assumptions of constant flux, constant SAR or constant initial activity, in those sedimentary scenarios where they would be properly applicable. The recent work by Abril and Brunskill (2014) showed that a statistical correlation between fluxes and SAR can be a quite general rule. The aim of this paper is to develop a new ^{210}Pb-based dating tool based on such correlation and the basic assumptions of continuity of the sequence, ideal deposition of fluxes and non post-depositional redistribution. The performance of the model is illustrated with a synthetic core, and with the study of two real cases of varved sediment taken from the scientific literature.

Abbreviations: TERESA, Time estimates from random entries of sediments and activities; SWI, sediment-water interface; SAR, mass sediment accumulation rate.

E-mail address: jmabril@us.es.

2. Material and methods

2.1. Time estimates from random entries of sediments and activities (TERESA) model

The model stands on the following set of assumptions: i) $^{210}Pb_{exc}$ behaves as a particle-associated tracer and new inputs are ideally deposited at the SWI over the previously existing material; ii) there is not any post-depositional redistribution; iii) continuity of the sequence (i.e., there is not any missing layer by erosion); iv) $^{210}Pb_{exc}$ fluxes are governed by 'horizontal inputs' (as defined in Abril and Brunskill, 2014). At the present stage the model will operate with continuous probability distributions for initial activities and SAR; and thus, it will be assumed that there are not any flood layers or other instantaneous inputs to the sediment column.

After coring, the standard method proceeds with the cutting of the sediment core into a certain number of slices. Each sediment slice (labelled with index i = 1,2, … N) is the result of the accumulated mass flow over a certain time interval ΔT_i. Let be w_i the average value of the mass flow into the SWI (SAR) over ΔT_i. For a sediment core composed by N slices, the magnitude $\overline{w}$ will be defined as the arithmetic mean of all w_i. Abril and Brunskill (2014) have shown that the values of w_i are distributed around $\overline{w}$ following approximately a normal distribution with standard deviation σ_w. These mass flows onto the SWI carry initial $^{210}Pb_{exc}$ activities, which similarly can be characterized by their mean value $\overline{A}_0$ and standard deviation σ_A. This random and independent variability naturally leads to a lack of correlation between initial activities and SAR, and it results in $^{210}Pb_{exc}$ fluxes ($F_i = A_{0,i}w_i$) that increase with SAR (Abril and Brunskill, 2014). This is summarized in Fig. 1. Thus, each sediment slice can be characterized by a pair of values ($A_{0,i}$, w_i).

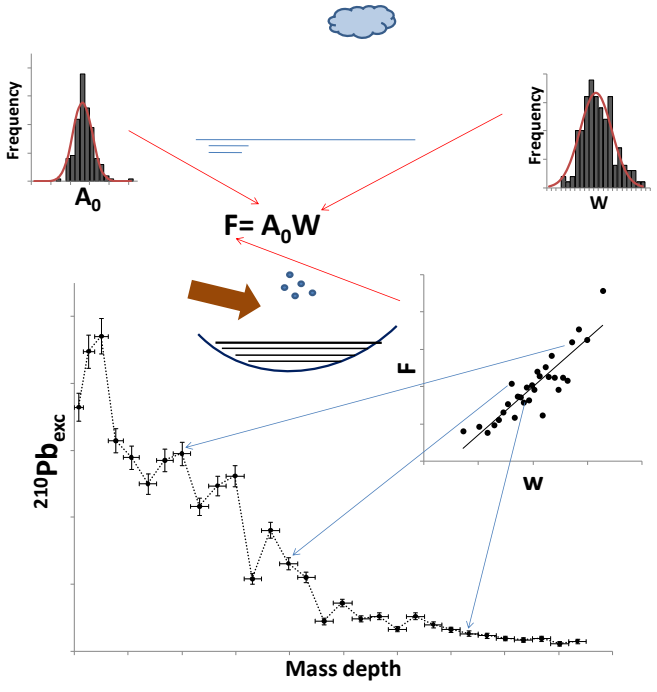

Fig. 1. Scheme with TERESA's model fundamentals. On the time scale associated to experimental sediment slices, the mass flow into the SWI (SAR, w) and its associate initial $^{210}Pb_{exc}$ activity (A_0) show a natural and independent variability that closely follow normal distributions. Consequently, the $^{210}Pb_{exc}$ fluxes (F) and SAR are linearly correlated. The sequence (or the sorting in time) of each pair of values of SAR and initial activity leads to the particular SAR history, the chronology and the $^{210}Pb_{exc}$ vertical profiles found in the sediment core.

These pairs occur in a certain order or sequence in time, what leads to the measured $^{210}Pb_{exc}$ profile (Fig. 1).

It will be helpful to introduce the relative deviations $s_w = \sigma_w/\overline{w}$; $s_A = \sigma_A/\overline{A}_0$. The first parameter had values of 0.30, 0.34, 0.27, 0.28, 0.32, 0.42, 0.24, 0.51 and 0.59 for the cores C1 to C9 studied by Abril and Brunskill (2014), while the second took values of 0.20, 0.25, 0.10, 0.43, 0.30, 0.29, 0.10, 0.15 and 0.22 for such cores C1 to C9, respectively.

The actual depth (with physical dimensions L) is not an appropriate magnitude due to compaction during the sediment accretion and to the shortening during the coring operation and later handling. The mass depth magnitude, m (with dimensions M L^{-2}), must be used instead. Data from the studied $^{210}Pb_{exc}$ versus mass depth profile will consists in a discrete set of N values of experimentally averaged specific $^{210}Pb_{exc}$ activities, $A_i(m)$, one for each sediment slice of mass thickness Δm_i, provided with their respective uncertainties, σ_i. Ages, T_i, will be referred at the bottom of each sediment slice, and SAR to their averaged values over the time interval associated to each slice. Thus, the experimental data can be arranged into a three column file with N triplets (m_i, A_i, σ_i). The mass depth magnitude (referred to the bottom of each slice) can be consistently handled within calculation for extracting the respective mass thickness intervals, and to calculate values referred to the centre of each slice.

Step 1. The model requires first-estimate values for $\overline{w}.\overline{A}_0$, and for their respective standard deviations (σ_w,σ_A). One possibility for achieving this goal is through an exponential fit (CF-CSR model) to the $^{210}Pb_{exc}$ vs. m profile; and by ascribing typical values of 35% and 20% for s_w and s_A, respectively.

Step 2. Generation of N random pairs of values for initial activities and SAR ($A_{o,i}$, w_i). A practical way for achieving this is to generate two sets of N values, $z_{1,i}$ and $z_{2,i}$, following normal typified distributions (this is, with mean value 0 and standard deviation 1.0). One can use the random number generator by Excel or others, but to avoid inaccuracies with low values of N, a systematic procedure is presented in Appendix A. The numbers within the series $z_{1,i}$, and a $z_{2,i}$ must be randomly ordered, and maintained during all the routine calculations. The pairs ($A_{o,i}$, w_i) will be then generated as follows:

$$\begin{aligned} A_{0,i} &= \overline{A}_0(1 + s_A z_{1,i}) \\ w_i &= \overline{w}(1 + s_w z_{2,i}) \end{aligned} \quad (1)$$

It can be tested that the fluxes $F_i = A_{0,i}w_i$ follow the expected trend of increasing with SAR. It will be assumed that the pairs ($A_{o,i}$, w_i) provide a reasonable proxy to the true values, and the question now is their appropriate ordering downcore.

Step 3. Sorting the pairs ($A_{o,i}$, w_i). As in a puzzle, one must decide which of these pairs is the best option for ascribing it to each particular sediment slice of index j (hereafter the index j = 1,2,… N will be used to refer the sequence of slices in the core, which is different from the initial and random ordering of pairs $A_{o,i}$, w_i). Their sorting leads to a chronology (the cumulative sequence of ΔT_i), and the application of corrections by radioactive decay transforms initial activities $A_{o,i}$ into the measured values at each sediment slice, A_j.

Treatment for the first sediment slice (j = 1). Let be $T_{up} = 0$ the age at the SWI. If the pair ($A_{o,k}$, w_k) − $k \in (1,N)$ denotes a particular value instead of a free index, was ascribed to the first slice, with a known mass thickness Δm_1, the age interval associated to this slice will be $\Delta T_1 = \Delta m_1/w_k$. Then, the expected (theoretical) averaged

value of the $^{210}Pb_{exc}$ specific activity in this layer, $A_{th,1}$, can be estimated from the involved hypothesis as

$$A_{th,1} = A_{0,k}\exp(-\lambda T_{up})\frac{1-\exp(-\lambda\Delta T_1)}{\lambda\Delta T_1}, \quad (2)$$

where λ is the radioactive decay constant for ^{210}Pb. This value can be compared against the measured one through the function $\Delta_1^2 = (A_{th,1} - A_1)^2$. The estimation will be repeated for all the pairs. The one that makes minimum Δ_1^2, will be selected as the best choice for the first layer. The corresponding pair ($A_{o,k}$, w_k) will be stored as the solution for this layer ($A_{o,1}$, w_1), and then excluded from the remaining set of pairs ($A_{o,i}$, w_i), now with i ranging from 1 up to N−1.

Treatment for the subsequent slices. For slice $j = 2$, the previous age T_{up} will be increased by $\Delta m_1/w_1$, and then the whole process will be repeated; and so on for the subsequent sediment slices. This way a chronology is generated as the required solution, along with the corresponding histories of SAR and flux onto the SWI. It is worth noting that the degree of freedom for selecting the best pair of values decreases downcore. Thus, it can be expected that the deepest part of the profile will be poorly described, but this is also the region of the core usually subject to the largest relative analytical errors.

Step 4. Generating parametric maps for the error function. The above solution is supported by the first estimates of $\overline{w}$, $\overline{A}_0$ and their respective relative standard deviations (step 1). The overall quality of the solution only can be evaluated from the measured profile, by using the typical error function:

$$Q^2 = \sum_{j=1}^{N}\left(\frac{A_{th,j} - A_j}{\sigma_j}\right)^2 ; \chi^2 = \frac{Q^2}{f}, \quad (3)$$

where f is the number of degrees of freedom (f = N- number of fitting parameters). The value of χ provides a measurement of the mean distance between the theoretical and the experimental profiles in terms of the size of the associated uncertainties.

Enough wide intervals can be defined for each initial parameter, centred on their first estimate values (step 1) and then scanned with any desired resolution. For each point in the previous 4-parametric grid, the whole process is repeated from steps 2 to 4, to generate the parametric maps of the χ function. The use of this function to find out the regions with suitable solutions will be discussed in more detail further below. The possibility of including independent time markers (reference points for the chronological line) to better constrict the model's answers will be also treated in the Results section.

Step 5. Error estimates for the reported results. The typical fundamentals can be applied for error estimates in the four entry parameters (namely $\overline{w}$, s_w, $\overline{A}_0$, s_A) through the curvature of the parametric lines in the Q^2 function around the position of the absolute minimum (Bevington and Robinson, 2003). The associated uncertainty to the age at the bottom of each layer, T_j, can be then estimated through the general propagation law:

$$\sigma^2(T_j) = \left(\frac{\partial T_j}{\partial \overline{A}_0}\sigma_A\right)^2 + \left(\frac{\partial T_j}{\partial \overline{w}}\sigma_w\right)^2 + \left(\frac{\partial T_j}{\partial s_A}\sigma(s_A)\right)^2 + \left(\frac{\partial T_j}{\partial s_w}\sigma(s_w)\right)^2 \quad (4)$$

The development of a friendly programming environment is out of the present scope of this work. Here, a set of numerical codes has been written with Quick-Basic. Excel sheets were used for generating random numbers and for plotting. Gnuplot and MATLAB also served for plotting and data handling.

2.2. Generation of synthetic cores for model testing

Two series of numbers $z_{1,i}$ and $z_{2,i}$ that follow normal typified distributions have been generated with N = 30 (see Appendix A and Table 1). The following parameter values have been selected: $s_A = 20\%$, $s_w = 30\%$, $\overline{A}_0 = 1000$ Bq kg^{-1}, $\overline{w} = 0.18$ g cm^{-2} y^{-1}. N pairs of ($A_{o,i}$, w_i) were then generated by using Eq. (1) (Table 1). The bulk density (with units of g cm^{-3}) has been modelled as $\rho(z) = 0.65 - 0.45\exp(-0.4z) + \delta(z)$, where δ(z) is a random noise with mean value 0.02 (this is a particular choice that handles realistic values and a typical depth profile). The synthetic core has been sliced at 1 cm intervals, and the respective mass thicknesses were estimated from the bulk density. The corresponding time intervals, ages, and the decay-corrected values of specific activities for each slice can be then estimated as described in step 3 (Methods section). The resulting $^{210}Pb_{exc}$ vs. mass depth profile appears in Fig. 2; and Table 1 reports the sequential stages for core construction as above described. It will be labelled as synthetic core SC-1. The associated uncertainties in $^{10}Pb_{exc}$ activities have been estimated as a 5%, plus a constant term of 5 Bq kg^{-1} (this last reproduces the effect of increasing relative uncertainties downcore).

From Table 1 it is possible to estimate the corresponding values of fluxes at the SWI, ($F_i = A_{o,i}\, w_i$), which follows the expected trend of increase with SAR ($R^2 = 0.789$), as shown in Fig. S-1 (in electronic supplementary material -ESM) for the normalized (to the arithmetic mean) values.

In real cores the distinct peak of ^{137}Cs, corresponding to the 1963 bomb fallout maximum, can be used as a time marker. In this synthetic core, the bottom of the sediment slice with $i = 14$ will be used for the same purpose, with an ascribed age of 48 ± 2 y.

It is worth noting that, independently of the particular way used for its construction, any $^{210}Pb_{exc}$ profile is compatible with an infinite number of chronological lines. In other words, there are always an infinite number of different chronologies and histories of SAR and fluxes that allows for the mathematically exact construction of the same $^{210}Pb_{exc}$ profile (Abril, 2015).

3. Results

3.1. Application of TERESA model to the synthetic core

3.1.1. Self-consistency tests

A numerical code has been developed to solve the TERESA model, following the method presented in Section 2.1. For testing the performance of the routine devoted to select the best ordering of pairs ($A_{o,i}$, w_i), the true values of $\overline{w}$, s_w, $\overline{A}_0$ and s_A for core SC-1 (Table 1) were used as entry parameters. Test-1 used as input file with typified distributions ($z_{1,i}$, $z_{2,i}$) the same arrangement of pairs used for generating the synthetic core (see Table 1). The code routine was able to find out the proper sequence downcore, with $\chi = 0.00$, and the exact solution for the chronology (Fig. 2). Test-2 used an independent and random rearrangement for ($z_{1,i}$, $z_{2,i}$) —see methodology in Appendix A; consequently only an approximate solution can be expected. This is, the numerical values of pairs ($A_{o,i}$, w_i) generated for model calculations are different from those used for generating the synthetic core, but the whole set represents a reasonable proxy. The solution, with $\chi = 0.71$, is shown in Fig. 2. This basic programming strategy will be referred hereafter as Method-A. Test-3 used the same input file than in Test-2, but it

Table 1
Data for synthetic core SC-1.

i	$z_{1,i}$	$z_{2,i}$	$A_{0,i}$ (Bq kg^{-1})	w_i (g cm^{-2} y^{-1})	Z (cm)	$\rho(Z)$ (g cm^{-3})	Δm (g cm^{-2})	m (g cm^{-2})	T (y)	A_i (Bq kg^{-1})	σ_i (Bq kg^{-1})
1	−1.192	−1.192	761.6	0.116	0.5	0.317	0.317	0.317	2.7	758	43
2	−0.784	0.126	1025.1	0.138	1.5	0.434	0.434	0.751	5.9	935	52
3	0.126	0.903	1180.5	0.187	2.5	0.512	0.512	1.262	8.6	975	54
4	−0.126	−0.674	865.1	0.173	3.5	0.557	0.557	1.819	11.8	656	38
5	−0.297	−0.573	885.4	0.164	4.5	0.597	0.597	2.416	15.5	607	35
6	1.036	−0.784	843.3	0.236	5.5	0.621	0.621	3.037	18.1	516	31
7	−0.042	0.297	1059.3	0.178	6.5	0.630	0.630	3.668	21.7	597	35
8	1.192	1.036	1207.3	0.244	7.5	0.652	0.652	4.320	24.3	609	35
9	0.042	−0.126	974.9	0.182	8.5	0.659	0.659	4.979	28.0	453	28
10	0.573	1.192	1238.4	0.211	9.5	0.653	0.653	5.632	31.0	514	31
11	2.128	2.128	1425.6	0.295	10.5	0.658	0.658	6.290	33.3	538	32
12	−1.383	−1.645	671.0	0.105	11.5	0.658	0.658	6.948	39.5	236	17
13	−0.674	1.645	1329.0	0.144	12.5	0.666	0.666	7.614	44.2	385	24
14	0.210	0.477	1095.4	0.191	13.5	0.662	0.662	8.277	47.6	275	19
15	−2.128	0.674	1134.9	0.065	14.5	0.667	0.667	8.944	57.9	256	18
16	0.297	−2.128	574.4	0.196	15.5	0.673	0.673	9.617	61.3	94	10
17	−0.477	0.210	1042.1	0.154	16.5	0.677	0.677	10.294	65.7	153	13
18	−1.036	−0.903	819.5	0.124	17.5	0.685	0.685	10.979	71.2	105	10
19	0.477	0.042	1008.4	0.206	18.5	0.673	0.673	11.652	74.5	109	10
20	−0.573	−1.383	723.4	0.149	19.5	0.674	0.674	12.326	79.0	71	9
21	1.383	1.383	1276.6	0.255	20.5	0.667	0.667	12.994	81.6	108	10
22	−0.210	0.385	1077.1	0.169	21.5	0.657	0.657	13.650	85.5	84	9
23	−0.385	−0.042	991.6	0.159	22.5	0.660	0.660	14.310	89.7	69	8
24	0.903	−0.477	904.6	0.229	23.5	0.668	0.668	14.978	92.6	55	8
25	−1.645	−0.297	940.7	0.091	24.5	0.674	0.674	15.652	100.0	52	8
26	−0.903	−0.385	922.9	0.131	25.5	0.682	0.682	16.334	105.2	41	7
27	0.674	−0.210	957.9	0.216	26.5	0.671	0.671	17.005	108.3	36	7
28	0.385	0.784	1156.7	0.201	27.5	0.678	0.678	17.683	111.7	40	7
29	0.784	−1.036	792.7	0.222	28.5	0.659	0.659	18.342	114.6	24	6
30	1.645	0.573	1114.6	0.269	29.5	0.664	0.664	19.006	117.1	31	7

$z_{1,i}$ and $z_{2,i}$ follow a normal typified distribution and are randomly sorted. They serve to construct values of initial activities, $A_{0,i}$ (with a mean value of 1000 and standard deviation of 20%), and SAR, w_i (with a mean value of 0.18 and standard deviation of 30%). Z is depth, measured down core, with origin at the SWI. $\rho(Z)$ is the bulk density, Δm the mass thickness of sediment slices 1 cm thick, and m the mass depth at the bottom of each slice, where ages, T, are also referred. A_i is the $^{210}Pb_{exc}$ specific activity, estimated as reported in Step 3 in the methods section, and σ_i the associated uncertainty (estimated as a 5% of relative error plus a constant term of 5 Bq kg^{-1}).

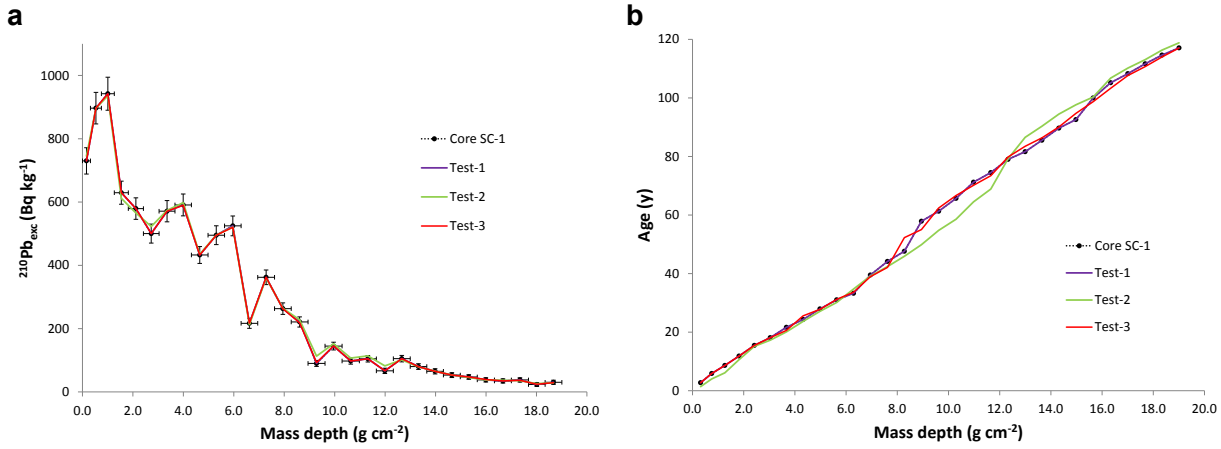

Fig. 2. a) $^{210}Pb_{exc}$ versus mass depth profile for the synthetic core SC-1 (Table 1). Vertical bars correspond to the associated uncertainties, while the horizontal ones define the mass depth interval of each sediment slice. The solutions generated by the numerical tests T1 to T3 (see text) are plotted as points at the centre of each slice interval (continuous lines are only for guiding-eyes). b) This panel depicts the corresponding chronological lines (estimated values for the bottom of each sediment slice).

applied a different programming strategy (Method-B): it is allowed comparing the suitability of a given $A_{o,i}$ value, combined with all the possible w_k values. The method should be able to reencounter the exact solution in this particular exercise (where the same numbers, although with a different ordering, have been used to generate the synthetic core). Nevertheless, it was sensitive to computational residuals, what can be overcome with a more robust mathematical code. In our case it provided a solution with $\chi = 0.09$ (Fig. 2).

3.1.2. *Estimates of entry parameters and mapping the χ function*

Although there may be other strategies, the CF-CSR model can be used to get, through an exponential fit to the $^{210}Pb_{exc}$ profile, a proxy to the parameter values for $\overline{w}$ and $\overline{A}_0$. It can be shown that the ability of this model to capture reliable "mean values" is limited by the way in which fluctuations in initial activities and SAR are distributed with time. For core SC-1, with a random distribution in SAR over time, the resulting values were 0.156 g cm^{-2} y^{-1} and 1033 Bq kg^{-1} for $\overline{w}$ and $\overline{A}_0$, respectively (with $R^2 = 0.95$).

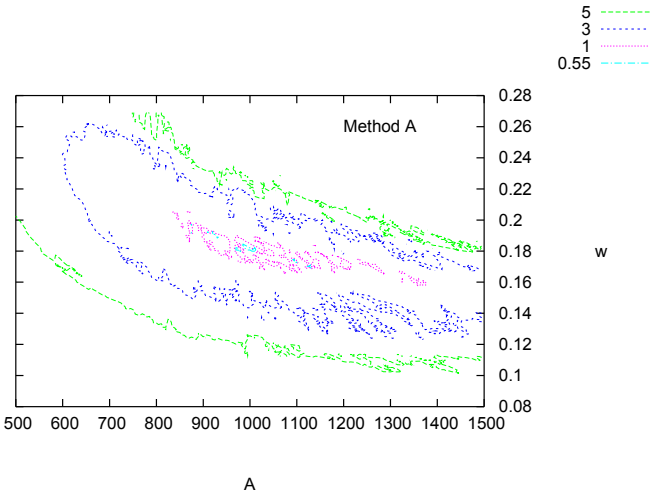

Fig. 3. Contour map for the function χ computed with method A as projected onto the planes ($\overline{A}_0$, $\overline{w}$), with relative resolution of 0.01 and maintaining the true values for the other two parameters (see Table 1).

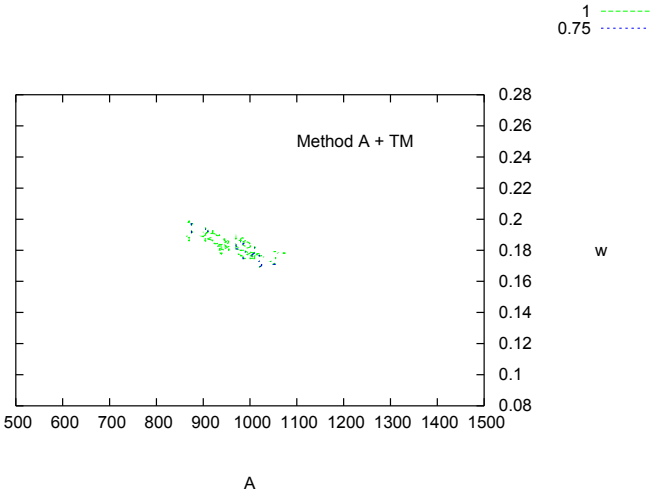

Fig. 4. Contour maps of Ω (Eq. (5)) for core SC-1 using a time mark (reference point) plotted in the ($\overline{A}_0$, $\overline{w}$) projection, as computed with method A.

Fig. 3 shows the contour map for the function χ computed with method A projected onto the planes ($\overline{A}_0$, $\overline{w}$) with relative resolution of 0.0,1and maintaining the true values for the other two parameters. In parallel, the projection onto the (s_A, s_w) plane can be handled (not shown). Although with a higher level of noise in method B (not shown), both methods were able to identify the minimum of χ around the true solution, but other secondary minima appeared in the surroundings, within the area of statistical significance of $\chi = 1$. The size of the region within a certain level of statistical significance must be put into the scope of the associated uncertainties in parameter values, and it can be constrained by using a time marker (a reference point in the chronological line).

3.1.3. The use of a time marker to constrain the model's answers

The time marker above discussed for core SC-1 provides an age T_m with an associated uncertainty σ_{T_m} for the bottom of the slice of index k_m. This has been used to define the following objective-function:

$$\Omega = \chi\left[1 + \left(\frac{T_{th}(k_m) - T_m}{\sigma_{T_m}}\right)^2\right] \quad (5)$$

A value of Ω close or lower than unity ensures that the solution reasonably fits the $^{210}Pb_{exc}$ profile and that the chronological line passes close to the time marker. Fig. 4 shows the corresponding contour map of Ω in the ($\overline{A}_0$,$\overline{w}$) projection, as computed with method A.

3.1.4. Error estimates for the entry parameters and for the resulting chronology

Following Bevington and Robinson (2003), the associated uncertainty σ_j for a parameter value a_j fixed by the criteria of minimizing the function Q^2 can be estimated from the curvature of the parametric line around the minimum:

$$\sigma_j^2 = 2\left(\partial^2 Q^2 \Big/ \partial a_j^2\right)^{-1}\Big|_{\min} \quad (6)$$

The code searches for the local minimum in the target region and calculates errors through Eq. (6). Results are shown in Table 2 for methods A and B. Finally, the associated uncertainty in the chronology can be estimated by Eq. (4). Results are shown in Fig. 5 for method A, and they are compared against the target chronology (Table 1).

3.1.5. SAR estimates

Due to the stochastic nature of the modelling approach, SAR values can deviate from the "true" ones, but compensating positive and negative deviations in the chronology, in such a way that this last does not deviate too much from the "true" solution. Only computed mean SAR values over a relatively wide time interval have some physical meaning. Fig. 6 shows the SAR values estimated by method A for each sediment slice in core SC-1, compared with the "true" SAR history (Table 1). The averaged values on a 5-slices basis are also depicted along with their respective deviations of the mean. These last compare well against the corresponding values in the "true" SAR history, but they only provide poor information on their temporal variations.

3.2. Application of TERESA model to real cases

3.2.1. Core C-1 (Santa Barbara Basin)

Table 3 reports data from a varved sediment core sampled at Santa Barbara Basin, at 34°14.0′N, 120°01.5′W and 575 m depth (Koide et al., 1972, 1973). The core, included in the compilation by Abril and Brunskill (2014), comprises 16 sediment slices. The $^{210}Pb_{exc}$ specific activity versus mass depth profile is plotted in Fig. 7. This data set will provide a suitable scenario for model testing.

Two typified normal distributions ($z_{1,i}$, $z_{2,i}$), with a random

Table 2
Determination of entry parameters and error estimates[a] for core SC-1.

	$\overline{A}_0$	$\overline{w}$	s_A	s_w	χ
Method A	990 ± 3	0.1800 ± 0.0002	0.220 ± 0.007	0.310 ± 0.002	0.42
Method B	1000.0 ± 0.9	0.1800 ± 0.0012	0.200 ± 0.010	0.300 ± 0.003	0.09

[a] Through the second derivative of the Q^2 function (Bevington and Robinson, 2003).

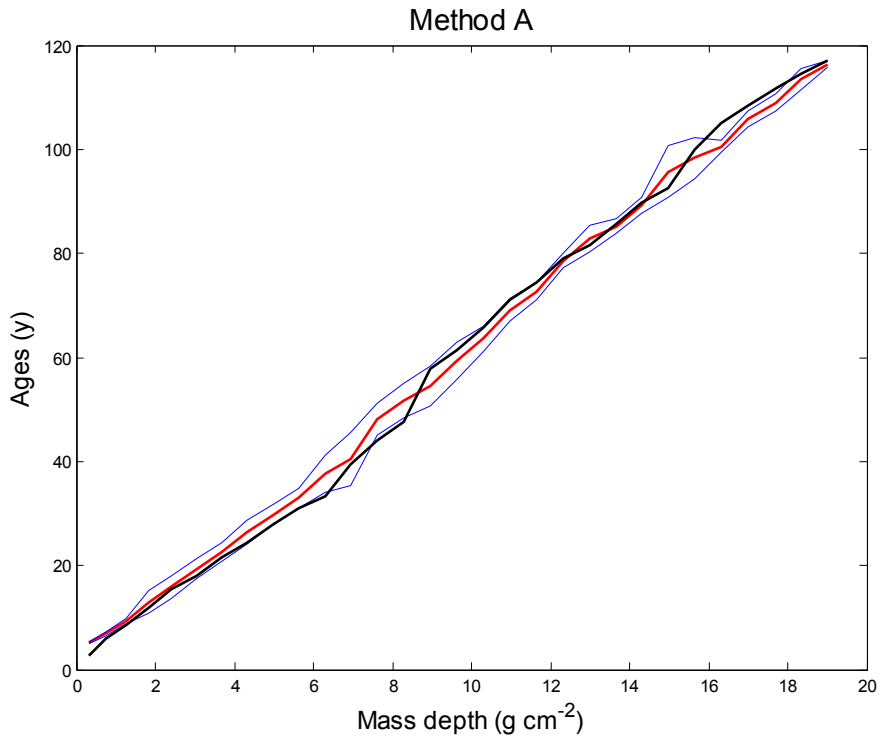

Fig. 5. Chronology estimated by TERESA model for core SC-1 by using method A along with the corresponding uncertainty intervals. The chronological line used to generate the synthetic core SC-1 (Table 1) is also depicted for the sake of comparison.

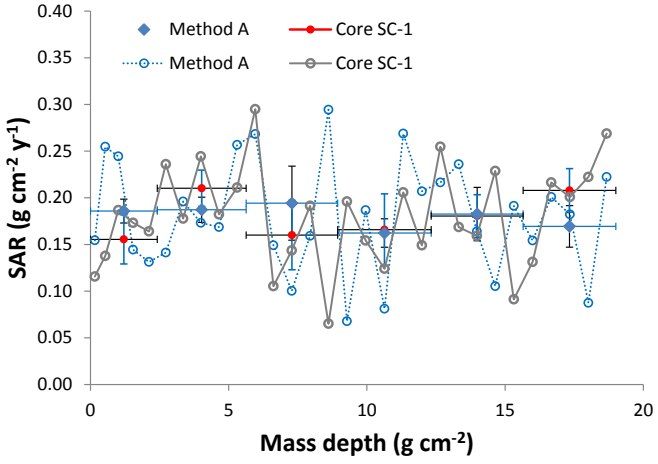

Fig. 6. SAR values estimated by method A for each sediment slice in core SC-1, compared against the "true" SAR history (Table 1). The averaged values on a 5-slices basis are also depicted along with their respective deviations of the mean.

Table 3
Data for Core C-1, Santa Barbara Basin (Koide et al., 1973).[a]

Depth (cm)	Dates (from varves)	SAR (g cm^{-2} y^{-1})	$^{210}Pb_{exc}$ (Bq kg^{-1})
0–1.6	1970–1971	0.146*	773 ± 26
1.6–3.2	1968–1970	0.150	1010 ± 30
3.2–4.8	1966–1968	0.146	960 ± 30
4.8–6.1	1964–1966	0.108	900 ± 30
6.1–7.1	1962–1964	0.089	803 ± 27
7.1–7.9	1960–1962	0.081	666 ± 23
7.9–8.7	1958–1960	0.076	546 ± 20
8.7–9.6	1956–1958	0.098	603 ± 22
9.6–10.3	1954–1956	0.080	710 ± 24
10.3–10.7	1952–1954	0.054	606 ± 22
10.7–11.2	1950–1952	0.071	545 ± 20
11.2–12.7	1945–1950	0.083	378 ± 16
12.7–15.0	1940–1945	0.121	353 ± 15
15.0–16.7	1935–1940	0.090	290 ± 13
16.7–18.1	1930–1935	0.093	356 ± 15
18.1–19.1	1925–1930	0.074	118 ± 10

[a] Core from Santa Barbara Basin; 34°14.0′N, 120°01.5′W; 575 m depth. Data from Table 1 in the original reference. Excess^{210}Pb was obtained by using a supported fraction of 3.5 ± 0.5 dpm g^{-1} (Koide et al., 1972) and counting errors of 3%. For each sediment slice, bulk density was estimated from water and organic matter contents reported in Table 1, allowing then for the determination of mass thickness (multiplying by the depth interval) and, finally, the corresponding SAR value (by using the interval of dates from varves). For the estimation of the first SAR value (noted with*) it has been assumed the date of sampling being ~1971.5. Although data for^{137}Cs are not available, to illustrate the use of the reference point technique, the equivalent 1963 time mark will be ascribed at the sediment slice at 6.1–7.1 cm depth.

rearrangement, have been generated with N = 16, following the methodology given in Appendix A. An exponential fit (CF-CSR model) provided the following first-estimate for the entry parameters: $\overline{A}_0 = 1175$ Bq kg^{-1}, $\overline{w} = 0.074$ g cm^{-2} y^{-1}, ($R^2 = 0.84$). For s_A and s_w, values of 20% and 30% were adopted as first-estimate, respectively. The pairs ($A_{o,i}$, w_i) were then generated from Eq. (1), and the resulting normalized fluxes increased with normalized SAR ($R^2 = 0.63$), as shown in Fig S-1 (ESM).

Fig. 8 shows the contour maps for χ and Ω, computed with the stand-alone method A. and with method A + TM (by using the 1963 time-marker), respectively. The method A has been applied then for accurately identifying the minimum in the target region and for estimating the associated uncertainties (Table 4). The resulting $^{210}Pb_{exc}$ profiles and the chronologies, these last with their corresponding propagated uncertainties, are shown in Figs. 7 and 9, respectively.

The greater complexity of method B (not shown) did not lead to better results than those from the more simple and straightforward method A. Additional tests did use a log-normal distribution for $A_{o,i}$

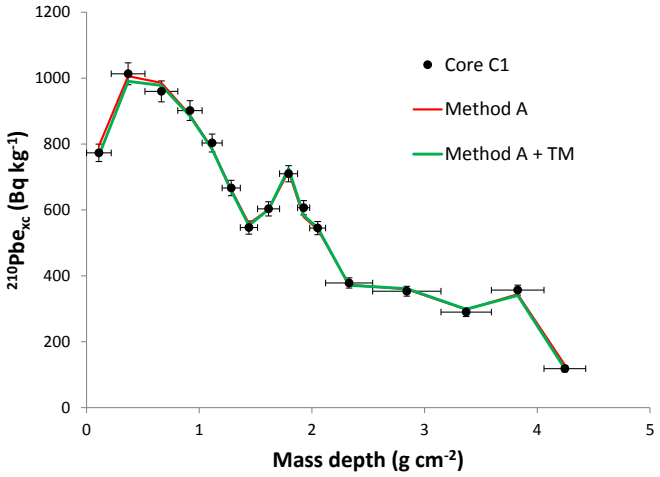

Fig. 7. $^{210}Pb_{exc}$ versus mass depth for core C-1 (Santa Barbara basin, see Table 3, with data from Koide et al., 1972, 1973). Vertical bars correspond to the associated uncertainties, while the horizontal ones define the mass-depth interval of each sediment slice. The continuous lines (with the same criteria for plotting than in Fig. 2) correspond to the solutions generated by TERESA model using methods A and A with the 1963 time mark.

instead of a normal one. The increased complexity in the programming did not lead to any improvement in model results (not shown).

Concerning SAR estimations, reference is made to the limitations above commented (only averaged values over relatively large time intervals are physically meaningful).

Core C-1 is of special interest, since it represents a great challenge for most of the existing ^{210}Pb-based dating models. For the sake of comparison, Fig. 10 plots the varve chronology (with a tentative value of 5% for the relative uncertainty –data not reported in the original reference) against the ones obtained with TERESA model (methods A and A + TM), and those generated by the application of several alternative models: CF-CSR, stand-alone CRS, and the CRS forced through the 1963 time mark.

i) CF-CSR model applies the common approach; it neglects the uppermost part of the sediment, until the ^{210}Pb maximum is attained, and uses an exponential fit. It provides a SAR value of w = 0.068 ± 0.007 g cm^{-2} year^{-1}.
ii) The stand-alone CRS model. As the measured inventory (23.7 kBq m^{-2}) is incomplete, this value was corrected by extrapolation of the exponential pattern found in the deepest layers, leading to an inventory correction of 3.6 kBq m^{-2}.
iii) CRS with the reference-point method. The CRS chronology is forced to match a reference time marker (the year 1963, in the layer 6.1–7.1 cm; see Table 1). The partial inventory contained in this top layer requires a constant flux of 1363 Bq m^{-2} year^{-1}. Assuming that this flux also holds for the deeper layers, one can easily estimate the correction which must be added to complete the inventory.

Details for the application of these last models can be found in Appleby (1998). As shown in Fig. 10, while the other models greatly deviated from the varve chronology, TERESA model was able to produce a reasonable estimate for ages.

3.2.2. *Core C-2 (Lake Sihailongwan)*

A second real case study uses the published data (in Table 5) for a varved sediment core sampled at Sihailongwan Lake (Northeast China, Jilin Province), 42°17′N, 126° 36′W; 50 m depth (Schettler et al., 2006a, 2006b). Authors reported a ^{137}Cs peak at the slice number 6. This slice corresponded to an age interval of 8 years, with mid point at 1972 (Table 5). Due to its low resolution, for the present modelling exercise an alternative time mark will be used instead. It will be ascribed at the centre of the slice number 7, with a varve date of 1964 (Table 5). This core was C-7 in the compilation by Abril and Brunskill (2014), where the reader is addressed for the statistical analysis. The corresponding $^{210}Pb_{exc}$ depth profile is shown in Fig. 11. The relative minimum in the slice number 5, which included several thick clastic layers, is likely due to episodic dust storms (Schettler et al., 2006b). The low $^{210}Pb_{exc}$ specific activities in dust particles produced anomalous low values in initial activities that deviated from the normal distribution (Abril and Brunskill, 2014).

The method in Appendix A allowed generating two typified normal distributions ($z_{1,i}$, $z_{2,i}$) with a random rearrangement for N = 21 (the number of sediment slices –see Table 5). The CF-CSR model provided $\overline{A}_0$ = 2145 Bq kg^{-1} and $\overline{w}$ = 0.020 g cm^{-2} y^{-1}, (R^2 = 0.983), while for s_A and s_w the first-estimate values of 20% and

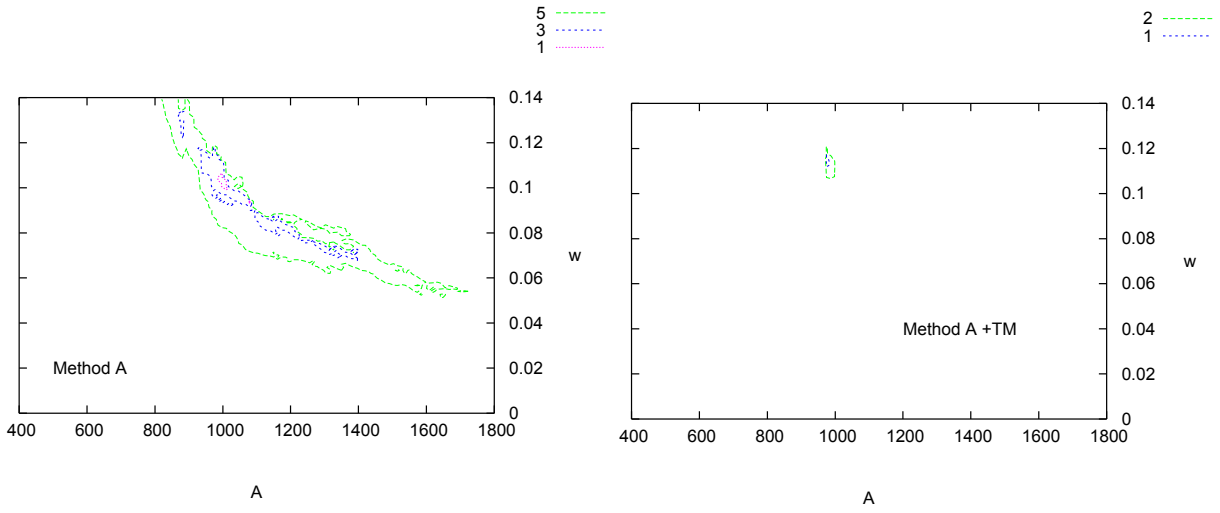

Fig. 8. Contour maps of the χ function for core C-1, generated by TERESA model using the stand-alone method A, and projected onto the plane ($\overline{A}_0$, $\overline{w}$). The second panel shows the contour map for the function Ω (Eq. (5)) using the 1963 time mark with method A. Values for S_A and S_W are given in Table 4.

Table 4
Determination of entry parameters and error estimates[a] for core C-1.

	$\overline{A}_0$	$\overline{w}$	s_A	s_w	χ
Method A	1003.0 ± 2.8	0.1030 ± 0.0016	0.190 ± 0.006	0.330 ± 0.018	0.71
Method A + TM	1000 ± 9	0.1110 ± 0.0019	0.200 ± 0.003	0.380 ± 0.013	0.53

[a] Through the second derivative of the Q^2 function (Bevington and Robinson, 2003).

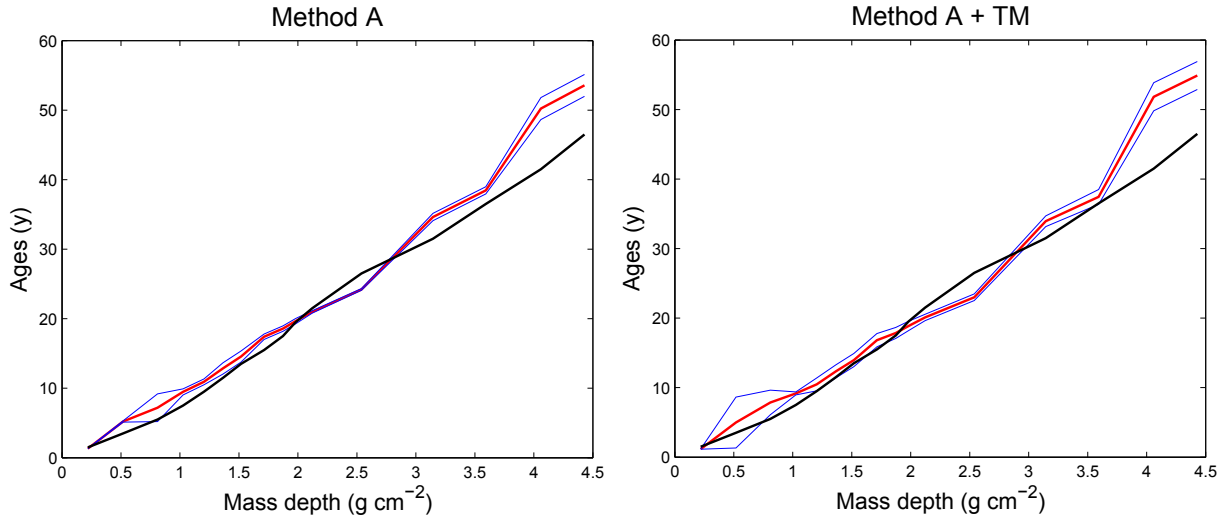

Fig. 9. Chronologies estimated by TERESA model for the core C-1 by using methods A, and A with the 1963 time-mark, along with their corresponding uncertainty intervals. The varve chronology (Table 3) is also depicted for the sake of comparison.

30% were adopted, respectively. Although not shown, the resulting normalized fluxes increased with normalized SAR ($R^2 = 0.71$).

Fig. 12 shows the contour maps for χ and Ω computed, after optimization, with the stand-alone method A and with the method A + TM, respectively. The stand-alone method A led to a poorly constrained solution, with a large area of statistical significance in the *A-w* plane containing several local minima. With the use of the time mark, the solution was reasonably good constrained around the values $\overline{A}_0 = 2250$ Bq kg^{-1} and $\overline{w} = 0.022$ g cm^{-2} y^{-1} (with $s_A = 0.31$; $s_w = 0.30$). For the sake of brevity, only this last case will

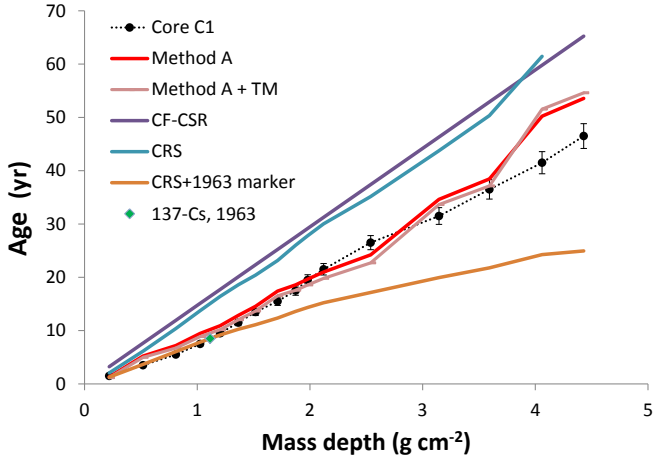

Fig. 10. Chronologies obtained with TERESA model for core C-1 by using methods A, and A with the 1963 time-mark (TM), compared against the varve chronology (Table 3, with a tentative value of 5% for relative uncertainties) and the chronologies produced by several alternative models: CF-CSR, stand-alone CRS, and CRS forced through the 1963 reference point.

Table 5
Data for Core C-2, Lake Sihailongwan (Schettler et al., 2006a)[a].

Depth (cm)	Dates (from varves)	SAR (g cm^{-2} y^{-1})	$^{210}Pb_{exc}$ (Bq kg^{-1})
0.5	1999	0.0092*	2411.8
1.5	1996.5	0.0094*	2415.0
2.5	1992	0.0115*	2167.0
3.5	1985.5	0.0225	1223.7
4.5	1979	0.0265	424.0
5.5	1972	0.0229	981.7
6.5	1964	0.0184	904.5
7.5	1953	0.0146	700.6
8.5	1942	0.0202	425.3
9.5	1930.5	0.0172	272.4
10.5	1919	0.0192	198.5
11.5	1907.5	0.0157	147.3
12.5	1893.5	0.0218	93.9
13.5	1879.5	0.0235	65.4
14.5	1866	0.0238	43.8
15.5	1851	0.0180	28.8
16.5	1836	0.0226	17.1
17.5	1821	0.0161	11.2
18.5	1804.5	0.0182	6.7
19.5	1790	0.0202	4.0
20.5	1776	0.0186	2.2

[a] Core from Sihailongwan Lake (Northeast China, Jilin Province), 42°17′N, 126° 36′W; 50 m depth. Sampled in September 1999. *Varves*: biogenic and clastic layers. Data from Tables 1 and 2 in Schettler et al. (2006a, Part 2); the latest include the author's estimation of $^{210}Pb_{exc}$ fluxes. See this reference for details on radioactive measurements and the involved uncertainties (here simplified as a 2% of relative error). Dates refer to the middle of the sample slices (±0.5–1.0 yr). SAR estimated from bulk density, slice thickness and age interval from varve counting, as reported in Schettler et al. (2006b, Part 1). As authors used freeze-core technology, the water content and solid density of the uppermost 3 cm (marked with*) could not be reliably measured (Schettler et al., 2006b). Authors reported a ^{137}Cs peak at the slice number 6. For the present modelling exercise a time mark will be ascribed at the bottom of sediment slice with a varve age of 40.5 yr.

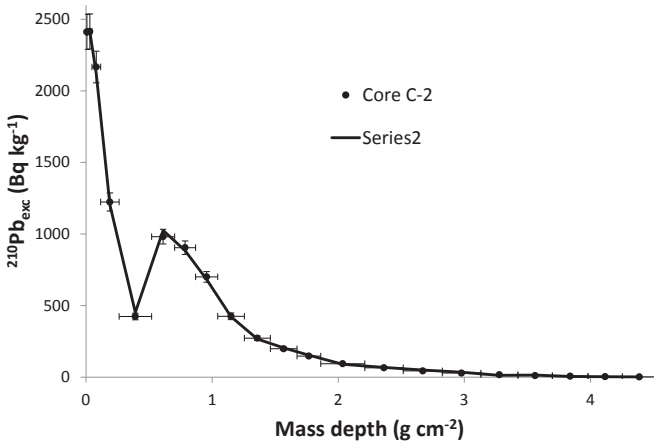

Fig. 11. $^{210}Pb_{exc}$ versus mass depth for core C-2 (Lake Sihailongwan, see Table 5, with data from Schettler et al., 2006a, 2006b). Vertical bars correspond to the associated uncertainties, while the horizontal ones define the mass-depth interval of each sediment slice. The continuous lines (with the same criteria for plotting than in Fig. 2) correspond to the solutions generated by TERESA model using method A with the 1964 time mark (see Table 5).

be analysed here. The method A has been applied then for accurately identifying the local minimum in the target region, and for estimating the associated uncertainties (in Table 6). The resulting $^{210}Pb_{exc}$ profile and the chronology are shown in Figs. 11 and 13, respectively. The propagated uncertainties in ages (not shown) were narrower than those found for core C-1. Again, TERESA model was able to identify a suitable solution through the technique of mapping the Ω function. The fit to the empirical $^{210}Pb_{exc}$ profile (Fig. 11) was quite good ($\chi = 0.85$), and the resulting chronology was reasonably close to the one obtained from varves (Fig. 13).

For the sake of comparison, Fig. 13 also plots the varve chronologies generated by the CF-CSR and the stand-alone CRS models. The first one applied the exponential fit to the whole data set. For the CRS model, the $^{210}Pb^{exc}$ inventory was corrected by extrapolation of the exponential pattern found in the deepest layers, leading to a small correction of 13.8 Bq m^{-2}. In this particular case, the application of the reference point method for forcing the CRS ages through the time mark was not possible, since it led to negative corrections for the total $^{210}Pb_{exc}$ inventory. Although the three models produced in this case close results, TERESA model behaved slightly better overall, and particularly for recent ages.

4. Discussion

Any $^{210}Pb_{exc}$ activity versus mass depth profile, independently of the precision in measurements, is compatible with an infinite number of chronological lines, being each one of them a mathematically exact solution for the history of initial activity, SAR and flux onto the SWI. From this infinite set of solutions, it is intended to extract a single one, or a very constrained set of solutions, which contain the statistical correlation between fluxes and SAR found by Abril and Brunskill (2014), since it seems to be a quite general rule for most of the sedimentary systems. TERESA model proposes a mathematical method for consistently generating a chronology from a $^{210}Pb_{exc}$ depth profile, by using such a statistical correlation. Several strategies (methods A, B, with normal and lognormal distributions) have been tested. Method A is the simplest and more straightforward one, what does not exclude the future development of more efficient tools.

Starting from initial estimates of the entry parameters (i.e., arithmetic mean values, over the N sediment slices, for initial activity, SAR, and their associated standard deviations), TERESA model generates tens of thousands (the mapping technique) of N doublets for initial activities and SAR that follow normal distributions. Then the code looks for the optimal ordering in time sequence of each of them to better fit the $^{210}Pb_{exc}$ profile (what is quantified through the χ function). The size of the region within a

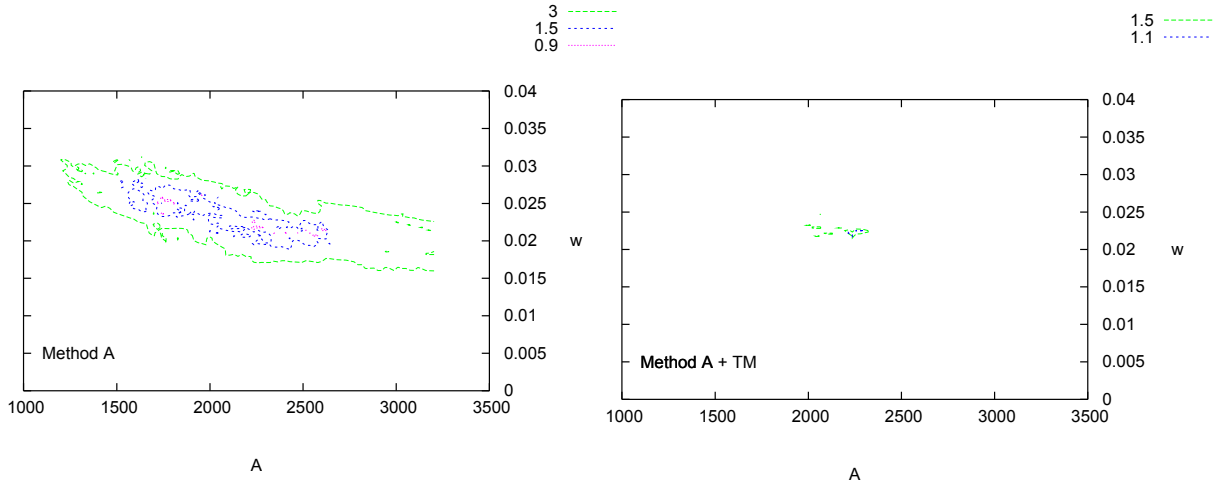

Fig. 12. Contour maps of the χ function for core C-2, generated by TERESA model using the stand-alone method A, and projected onto the plane ($\overline{A}_0$, $\overline{w}$). The second panel shows the contour map for the function Ω (Eq. (5)) using the 1964 time mark with method A. Values for s_A and s_W are given in Table 6.

Table 6
Determination of entry parameters and error estimates[a] for core C-2.

	$\overline{A}_0$	$\overline{w}$	s_A	s_w	χ
Method A + TM	2245 ± 2	0.0227 ± 0.0001	0.310 ± 0.002	0.300 ± 0.003	0.85

[a] Through the second derivative of the Q^2 function (Bevington and Robinson, 2003).

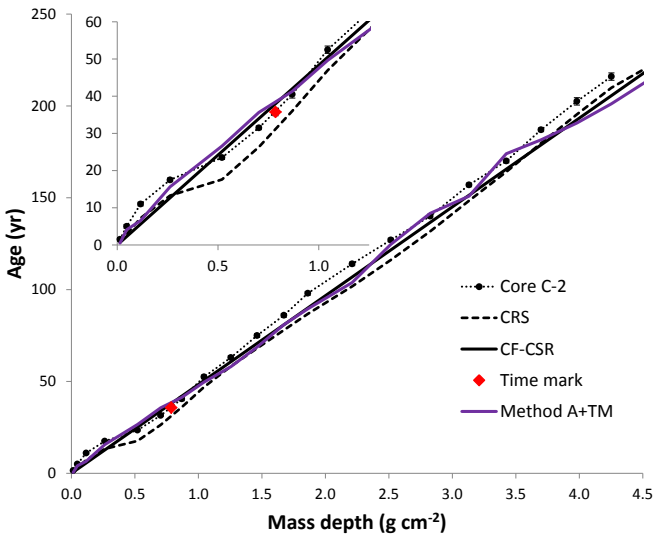

Fig. 13. Chronologies obtained with TERESA model for core C-2 by using method A with the 1964 time-mark (TM), compared against the varve chronology (Table 5), and the chronologies produced by the CF-CSR and the stand-alone CRS models. The figure contains a subpanel with a zoom to the younger sediment slices.

certain level of statistical significance in the parametric *A*-*w* plane was large in the three examples. For core C-1 it was possible to localize a relatively well defined absolute minimum leading to a well constrained solution. Nevertheless, for the synthetic core and for core C-2, there appeared several local minima. It is necessary to gain experience with the application of TERESA model to a wider data set, to identify what are the special characteristics of a $^{210}Pb_{exc}$ profile that lead to a well defined absolute minimum in the χ function.

TERESA model allows for the use of a time mark to better constrain the model's answers. Although there may be other programming strategies, the present work used the objective function Ω (Eq. (5)). In the three studied cases, it was possible to identify a well constrained solution, with the resulting chronologies being in reasonably good agreement with the "true" ones (synthetic data or varved chronologies). Again, it is necessary to gain experience to learn about the limitations of this technique.

It is worth noting the model capability to account for some episodic events, as the atypical low values for initial activities associated to the dust storms that affected to core C-2. Thus, in this case the model identified a higher value for s_A (Table 6).

The method used for estimating the associated errors in the entry parameters led to relatively narrow uncertainty intervals. The same is true for the chronology. This result must be interpreted in terms of model sensitivity. Deviations from the true solution cannot be explained only in terms of uncertainties in the entry parameters, since they also involve "model errors". The generation of random numbers leads to distributions of initial activities and SAR values that only can be a proxy to the real ones. As these last are unknown, there makes no sense to play with alternative distributions, since there is no way to distinguish which of them better fits the real situation (when a varve chronology is not available).

CRS and CF-CSR models assume the constancy of fluxes onto the SWI. Their mathematical formulation allows compensating to some extend the positive and negative deviations from the true chronology. This happens when positive and negative fluctuations in fluxes are well distributed in time (Abril and Brunskill, 2014), and this is roughly the case of core C-2. Core C-1 concatenates 5 sediment slices with an strong increase in $^{210}Pb_{exc}$ fluxes onto the SWI ($F = A_0 w$ in Table 1, or see figures in Abril and Brusnkill, 2014). Thus, models CF-CSR and CRS (including for this latest the reference point method) fail to account for the varve chronology. It has been shown how TERESA model is able to provide reasonable age estimates in the three studied cases, what does not imply its ability for generating high resolution SAR histories. It is worth noting that this last is also true for CRS, SIT and other chronological models.

5. Conclusions

Previous works have shown that a correlation between flux and SAR is a quite common situation in sedimentary systems. TERESA is a ^{210}Pb-based dating model for recent sediments that uses the previous statistical correlation along with the assumptions of ideal deposition, continuity of the sequence and non post-depositional redistribution. The performance of the model has been tested with a synthetic core, and with two real case studies using published data for varved sediment cores. Particularly, for core C-1, while other models greatly deviated from the varve chronology, TERESA model was able to produce a reasonable estimate for ages.

TERESA model is a promising dating tool that, at least partially, could overcome some of the difficulties found with the classical restrictive assumptions used in other ^{210}Pb-based dating models. Nevertheless it is necessary to gain experience with its application to a wider data set in order to learn about its potentials and limitations.

Acknowledgements

This work was funded partially by the FIS2012-31853 Project.

Appendix A

Random numbers generation

To generate N values for z_i following a normal typified distri-bution, one can split the distribution into N intervals over which the integral probability is $p = 1/N$. When N is pair, the first point, z_1, in the positive branch of the distribution verifies that the cumulative probability in the interval $(-\infty, z_1)$ is $\frac{1}{2}+p/2$; for z_2 the previous cumulative probability increases by p, and so on up to $z_{N/2}$. A symmetric distribution is generated for the N/2 negative numbers. When N is an odd number, $z_1 = 0$, and the (N-1)/2 positive series is generated with the same method, and similarly for the $(N-1)/2$ negative set. The DISTR.NORM.INV function of excel can be used to find out the corresponding values for z_i. These numbers must now be randomly sorted. A practical way for doing this is to generate with Excel a column with N random numbers following a normal distribution, beside the previous z_i series, and to use then the function of sorting from minor to major with the option of extending the selection range.

References

Abril, J.M., Brunskill, G.J., 2014. Evidence that excess ^{210}Pb flux varies with sediment accumulation rate and implications for dating recent sediments. J. Paleolimnol. 52, 121–137.

Abril, J.M., 2015. Why would we use the Sediment Isotope Tomography (SIT) model to establish a 210Pb-based chronology in recent-sediment cores? J. Environ. Radioact. 143, 40–46.

Appleby, P.G., 1998. Dating recent sediments by ^{210}Pb: problems and solutions. In:

Illus, E. (Ed.), Dating of Sediments and Determination of Sedimentation Rate, pp. 7—24. STUK A-145, Finland.
Appleby, P.G., 2008. Three decades of dating recent sediments by fallout radionuclides: a review. Holocene 18, 83—93.
Bevington, P.A., Robinson, D.K., 2003. Data Reduction and Error Analysis for the Physical Sciences, third ed. McGraw-Hill, New York.
Carroll, J., Lerche, I., 2003. Sedimentary Processes: Quantification Using Radionuclides. Elsevier, Oxford.
Koide, M., Soutar, A., Goldberg, E.D., 1972. Marine geochronology with ^{210}Pb. Earth Planet. Sci. Lett. 14, 442—446.
Koide, M., Bruland, K., Goldberg, E.D., 1973. Th-228/Th-232 and Pb-210 geochronologies in marine and lake sediments. Geochim. Cosmochim. Acta 37, 1171—1187.
Mabit, L., Benmansour, M., Abril, J.M., Walling, D.E., Meusburger, K., Iurian, A.R., Bernard, C., Tarján, S., Owens, P.N., Blake, W.H., Alewell, C., 2014. Fallout ^{210}Pb as a soil and sediment tracer in catchment sediment budget investigations: a review. Earth-Sci. Rev. 138, 335—351.
Ojala, A.E.K., Francus, P., Zolitschka, B., Besonen, M., Lamoureux, S.F., 2012. Characteristics of sedimentary varve chronologies— a review. Quat. Sci. Rev. 43, 45—60.
Sánchez-Cabeza, J.A., Ruíz-Fernández, A.C., 2012. ^{210}Pb sediment radiochronology: an integrated formulation and classification of dating models. Geochim. Cosmochim. Acta 82, 183—200.
Schettler, G., Mingram, J., Negendank, J.F.W., Jiaqi, L., 2006a. Paleovariations in the East-Asian Monsson regime geochemically recorded in varved sediments of Lake Sihailongwan (Northeast China, Jilin province). Part 2: a 200-year record of atmospheric lead-210 flux variations and its palaeoclimatic implications. J. Paeolimnol. 35, 271—288.
Schettler, G., Qiang, L., Mingram, J., Negendank, J.F.W., 2006b. Paleovariations in the East-Asian Monsson regime geochemically recorded in varved sediments of Lake Sihailongwan (Northeast China, Jilin province). Part 1:Hydrological conditions and flux. J. Paleolimnol. 35, 239—270.